J. Am. Ceram. Soc., 1–7 (2016)
DOI: 10.1111/jace.14262

journal

Sustainable Method for the Large-Scale Preparation of Fe_3O_4 Nanocrystals

SungWoo Lee,[‡] Jae-Sik Yoon,[§] Sungkyoung Kang,[¶] Kihyun Kwon,[‖] Ki Soo Chang,[§] SangGap Lee,[§] Sang-Il Choi,[‡‡] Jong-Ryul Jeong,[‡,†] Gaehang Lee,[§,†] and Ki Min Nam[§§,†]

[‡]Department of Materials Science and Engineering and Graduate School of Energy Science and Technology, Chungnam National University, Daejeon 305-764, Korea

[§]Korea Basic Science Institute(KBSI), Daejeon 305-806, Korea

[¶]Department of Chemistry, Korea Advanced Institute of Science and Technology (KAIST), Daejeon 305-701, Korea

[‖]R&D Center, Kumho Petrochemical, Daejeon 305-348, Korea

[‡‡]Department of Chemistry and Green-Nano Materials Research Center, Kyungpook National University, Daegu 702-701, Korea

[§§]Department of Chemistry, Mokpo National University, Jeonnam 534-729, Korea

In this work, a facile synthetic process is reported for the large-scale synthesis of Fe_3O_4 nanocrystals. Thermal decomposition of $Fe(acac)_3$ (100 g) in 1-hexadecanol produced Fe_3O_4 nanocrystals with well-controlled sizes and morphologies. The nanocrystals were spherically shaped with average diameters of 7.8 ± 0.6, 6.5 ± 0.4, and 5.9 ± 0.2 nm when prepared at 300°C, 270°C, and 250°C, respectively. Mechanisms of crystal formation were elucidated on the basis of gas chromatography-mass spectroscopy analysis, enabling the large-scale preparation of Fe_3O_4 nanocrystals. To provide an environmentally benign route, Fe_3O_4 nanocrystals were prepared with recycled solvent which was recovered from the initial experiment. The resulting porous Fe_3O_4 nanocrystals had larger average sizes than those of the initial nanocrystals. Structural characterization was performed using transmission electron microscopy and powder X-ray diffraction.

Keywords: *large-scale preparation; economical method; iron oxides; nanomaterials*

I. Introduction

Metal oxide nanocrystals have attracted great interest because they can be used as catalysts, battery materials, electrical devices, and gas sensors.[1–3] The wet chemical method for the production of monodisperse nanocrystals, involving nucleation and growth of particles in solution, has been well-established for several decades.[4] For practical use, many metal oxides have been synthesized via hydrolysis and condensation of reagents in an aqueous solution.[5,6] These processes have also been successfully adapted for nanocrystal synthesis. However, hydrolytic processes suffer from a few major drawbacks, such as low crystallinity and poor size control of particles despite extensive efforts for improvement because of the complexity of the aqueous reaction conditions. A large-scale process with high product quality is still required for future technological applications as well as fundamental scientific interest.

Iron oxide nanocrystals have been studied extensively because of their catalytic and magnetic properties.[2,7] Previously, our group also demonstrated the synthesis and characterization of Fe_3O_4 nanocrystals using nuclear magnetic resonance (NMR) spectroscopy and X-ray diffraction (XRD).[8,9] However, elucidation of the formation mechanisms in a nonhydrolytic system remains challenging. The development of plausible synthetic mechanisms should enable the preparation of targeted compounds with controlled sizes in a predicted manner.

In this work, a facile synthetic process is reported for the large-scale synthesis of Fe_3O_4 nanocrystals. Thermal decomposition of $Fe(acac)_3$ (acac = acetylacetonate) in 1-hexadecanol produced Fe_3O_4 nanocrystals with controlled sizes and morphologies. Crystal formation mechanisms were elucidated based on gas chromatography-mass spectroscopy (GC-MS) analysis, enabling the large-scale production of Fe_3O_4 nanocrystals. Structural characterization was performed using transmission electron microscopy (TEM) and XRD. Moreover, porous Fe_3O_4 nanocrystals were prepared using recycled solvent, which was recovered from a previous process to demonstrate the feasibility of a practical application. The resulting Fe_3O_4 nanocrystals had larger average sizes and pores. Because 1-hexadecanol could be used repeatedly without the generation of waste, the entire process economically consumed reagents. This synthetic method had a high yield, good reproducibility, and convenient processing procedures, enabling large-scale industrial applications.

II. Experimental Procedure

(1) Materials

$Fe(acac)_3$ (97%) and 1-hexadecanol (99%) were purchased from Sigma Aldrich (St. Louis, MO) and used without further purification. Ethanol (99.5%) and toluene (99.5%) were purchased from Daejung Chemicals (Shiheung, Korea).

(2) Preparation of Fe_3O_4 Nanocrystals for GC-MS Analysis

$Fe(acac)_3$ (2 g) and 1-hexadecanol (8.18 g) were vigorously stirred in a 50 mL glass vial at 80°C for 1 h in an ambient air atmosphere. The reaction mixture was heated to 300°C (with a 30 min ramp time) and held at this temperature for 30 min. The resulting black-brown reaction mixture was cooled to room temperature before ethanol (30 mL) was

P. Davies—contributing editor

Manuscript No. 38092. Received January 29, 2016; approved March 21, 2016.
S. W. Lee and J.-S. Yoon contributed equally to this work.
[†]Authors to whom correspondence should be addressed. e-mails: namkimin.chem@gmail.com, ghlee@kbsi.re.kr and jrjeong@cnu.ac.kr

added. The suspension was then centrifuged, and the supernatant was collected to study the mechanism of the formation of Fe_3O_4 (magnetite) nanocrystals.

(3) Large-Scale Synthesis of Fe_3O_4 Nanocrystals

A mixture of $Fe(acac)_3$ (100 g) in 1-hexadecanol (409 g) was prepared in a 2 L glass beaker. This mixture was stirred at 80°C for 1 h in an ambient air atmosphere. The solution was then heated to 300°C (with a 30 min ramp time) and held at this temperature for 30 min, yielding a black-brown dispersion (See Figs. S1 and S2). The resulting solution was cooled down to room temperature and centrifuged to collect the supernatant for recycling the solvent. Then, the precipitates were washed three times with toluene (50 mL) and ethanol (150 mL) to remove excess reactants and byproducts. The nanocrystals were spherically shaped with an average diameter of 7.8 ± 0.6 nm. Synthetic and purification procedures analogous to those reported above resulted in Fe_3O_4 nanocrystals with diameters of 6.5 ± 0.4 and 5.9 ± 0.2 nm at reaction temperatures of 270°C and 250°C, respectively.

(4) Economical Preparation of Porous Fe_3O_4 Nanocrystals

$Fe(acac)_3$ (100 g) and recycled solvent from the experimental procedure (3), the first supernatant, were mixed in a 2 L flask at 80°C for 1 h. The reaction mixture was then heated to 300°C (with a 30 min ramp time) and maintained at this temperature for 30 min. The resulting black-brown reaction mixture was cooled to room temperature and centrifuged to collect the supernatant for the second recycling of the solvent. The precipitates were washed three times with toluene (50 mL) and ethanol (150 mL) to provide porous Fe_3O_4 nanocrystals. The resulting porous nanocrystals were quasi-cube shaped with an average diameter of 25 ± 2.7 nm. When this recycling procedure was conducted again with $Fe(acac)_3$ (100 g) and recollected solvent, the second supernatant, porous Fe_3O_4 nanocrystals were formed with a diameter of 36 ± 3.2 nm.

(5) Material Characterization

The crystal phase of Fe_3O_4 nanocrystals was characterized by powder XRD using a Bruker AXS D8 ADVANCE diffractometer equipped with a Linxeye 1-D detector (Bruker AXS GmbH, Karlsruhe, Germany), with a CuK_α radiation source (40 kV and 40 mA), $2\theta = 20°$ and 80°, a divergence angle of 0.2°, a step size of 0.02°, and an acquisition time of two-seconds per step. Rietveld refinement was performed using the TOPAS software package (ver. 4.2, Bruker AXS 2005) while implementing the fundamental parameters approach (FPA).[10,11] The FPA was based on a convolution profile-fitting process. Profile shape calculations were performed, and intensity profiles were generated based on the standard instrumental parameters using the FPA implemented in the TOPAS program. The results were fit to a LaB6 standard measurement, which was synthesized from the emission profile, the specimen-dependent parameters, and the instrument parameters. The background was fit using the user-specified number of coefficients of a Chebychev polynomial, and "Crystallite size" and/or "Microstrain" parameters were used to model microstructure-controlled line broadening.[12,13] The Rietveld analysis generates R factors, e.g., $R_{exp,}$ which were found to be large. The R factors were $R_{exp} = 10.54\%$, $R_{wp} = 11.05$, $R_p = 8.77$, and GOF = 1.05 (Table S1). A low value of χ^2 (goodness of fit) was refined, justifying the reasonable refinement value. TEM images, high-resolution TEM (HR-TEM) images, and electron-diffraction patterns of Fe_3O_4 nanocrystals deposited on a carbon-coated Cu grid were observed using a transmission electron microscope, TEM, (JEOL JEM-2100, Tokyo, Japan) operated at 200.0 kV. Image acquisition and size calculations were performed using the iTEM software package (Olympus Soft Imaging Solutions, Münster, Germany). Images were recorded with a charge-coupled device camera (MegaView, Olympus Soft Imaging Solutions).

Quantitative analysis of the solvent (1-hexadecanol) and supernatants from the reaction mixtures was performed using a gas chromatograph coupled with a mass spectrometer (GC Clarus 600/MS Clarus 600T, Perkin Elmer). The gas chromatograph was equipped with a capillary column, Elite-5MS (Perkin Elmer, Waltham, MA, 30 m length, 0.25 mm inner diameter, and 0.25 μm film thickness). The mass spectrometer was configured for electron impact ionization mass spectrometry (EI-MS) at 70 eV. The interface and source temperature were both 250°C. The temperature of the column was controlled by following a temperature program such that the column temperature was ramped at 10°C/min from 50°C to 280°C and maintained at 280°C for 2 min. Magnetic properties of the products were measured at room temperature with a vibrating sample magnetometer (VSM, 7004, Lake Shore, Westerville, OH) with an applied field between −10000 and 10000 Oe.

III. Results and Discussion

(1) Reaction Mechanism for the Formation of Fe_3O_4 Nanocrystals

Synthetic processes for the preparation of monodisperse nanocrystals are relatively well-established.[14] Unfortunately, most of the synthetic methods considered to date have only focused on the quality of the nanocrystals produced. An understanding of synthetic mechanisms would enable the preparation of targeted compounds with controlled sizes in a predictable fashion.[15,16] The Fe_3O_4 nanocrystals have been prepared by using 1-hexadecanol not only as a reactant but also as a surfactant. Analysis of the side products helps us to understand the detailed formation mechanism of Fe_3O_4 nanocrystals. GC-MS was used to investigate the mechanism of the chemical reaction of $Fe(acac)_3$ and 1-hexadecanol under ambient atmospheric conditions. When the synthesis of Fe_3O_4 was complete, the reaction mixture was centrifuged. The supernatant was collected and analyzed by GC-MS. Four side products were identified by comparison to the reference peaks shown in Fig. 1, which included (1) 16-hydroxyhexadecanoic acid, (2) 4-hydroxy-5-methyl-pentan-2-one, (3) 1-hexadecanol, (4) 1-hexadecanyl acetate. Species (1) is an

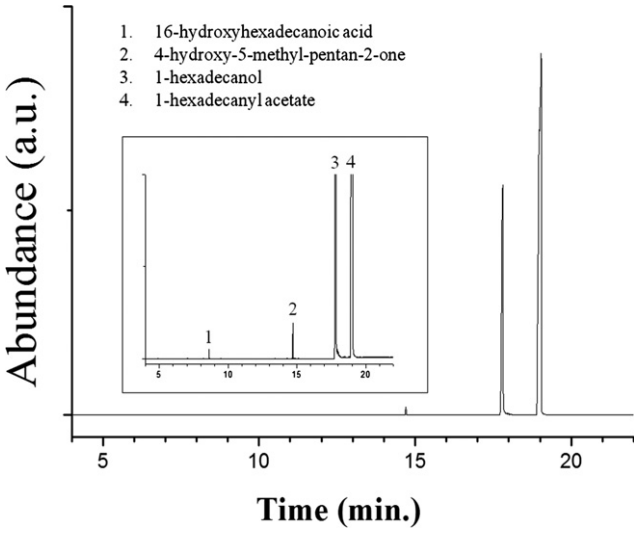

Fig. 1. Gas chromatogram of the supernatant from the reaction mixture for the preparation of Fe_3O_4 nanocrystals. The products are as follows: (1) 16-hydroxyhexadecanoic acid, (2) 4-hydroxy-5-methyl-pentan-2-one, (3) 1-hexadecanol, (4) 1-hexadecanyl acetate. The enlarged chromatogram is shown in the inset.

impurity in 1-hexadecanol (Fig. S3). Species (2) and (4) are side products of the decomposition of $Fe(acac)_3$. Plausible reaction pathways for the formation of Fe_3O_4 nanocrystals, based on solvolysis and condensation, are given in Fig. 2. 1-hexadecanol undergoes a nucleophilic attack of a carbonyl carbon atom in the acac ligand.[17] The C–C bond between the carbonyl carbon and the center carbon was broken, forming species (4) and acetone through alcoholysis. Acetones underwent an aldol reaction with the iron center, forming species (2). The resulting Fe–OCH_2R species reacted with other Fe compounds to form Fe–O–Fe bonds, and the continuous formation of the Fe–O bonds by the thermal decomposition led to the generation of Fe_3O_4 seeds.[18] During the thermal decomposition process of $Fe(acac)_3$, 1-hexadecanol decomposed to 4-hydroxy-5-methyl-pentan-2-one and 1-hexadecanyl acetate, which produced reductive environments.[19–22] The reduction of $M(acac)_3$ (M = Fe, Co, Mn) induced by oxidative decomposition of surfactants was studied well in the literature.[19,20] Furthermore, the formation mechanisms of oxygen-deficient metal oxides by heating in a reductive environment were also well-known.[15] Thus, the reduction of Fe^{3+} to Fe^{2+} has been explained by oxidative decomposition of 1-hexadecanol, i.e., dehydrogenative oxidation of 1-hexadecanol,[21,22] which is responsible for the formation of Fe_3O_4 with a mixed valence ($(Fe^{2+}{}_{1/3}Fe^{3+}{}_{2/3})_3O_4$, magnetite phase) using only an Fe^{3+} precursor in these synthetic conditions.

(2) Large-Scale and Economical Preparation of Fe_3O_4 Nanocrystals

To scale-up the preparation of Fe_3O_4 nanocrystals, $Fe(acac)_3$ (100 g) and 1-hexadecanol (409 g) were mixed in a 2 L beaker, which was heated to 300°C (with a 30 min ramp time) and maintained at this temperature for 30 min. The amount of nanocrystals produced was as large as 20.3 g with a yield of 93% compared to the theoretical yield of 21.9 g [Fig. S2 (a)]. The nanocrystals were well dispersed in toluene and easily attracted to a magnet [Figs. S2(b) and (c)]. Figure 3(a) and S4(a) show TEM images of the monodispersed Fe_3O_4 nanocrystals, which were spherically shaped with an average size of 7.8 ± 0.6 nm. The fast flourier transformation (FFT) and selected area electron-diffraction (SAED) patterns were identical to those of the magnetite phase [Figs. 3(a) and S5]. The lattice spacing of Fe_3O_4, which is shown in the high-resolution HRTEM image in Fig. 3(b), was approximately 0.254 nm ((311) plane), which corresponded to that of a highly crystalline nature with a well-defined nanocrystal morphology. Reaction temperatures of 270°C and 250°C yielded monodispersed nanocrystals with average diameters of 6.5 ± 0.4 and of 5.9 ± 0.2 nm, respectively (Figs. 3 and S4), indicating that the scale-up processes were successfully demonstrated.

In order to obtain a reliable structural description of this material, Rietveld analysis was performed on nanocrystals with a diameter of 7.8 ± 0.6 nm (Fig. S6). The diffraction pattern was indexed by the *Fd*-3*m* space group (magnetite, JCPDS No. 71-6336) with a lattice parameter, $a = 8.3842$ (13) Å, which confirmed the successful synthesis of Fe_3O_4 nanocrystals. Figure 4 shows the XRD patterns of the various Fe_3O_4 nanocrystals assigned to the standard magnetite phase. Crystallite sizes from the (311) diffraction peaks using the Debye–Scherrer equation were also determined to be 7.9, 6.8, and 6.1 nm. These values were in agreement with the particle sizes obtained from TEM images. Because $Fe(acac)_3$ and 1-hexadecanol are only used in an ambient air atmosphere, the entire process is economically facile. Overall synthetic cost is comparable with that of the Fe-oleate decomposition process.[14]

Moreover, it is more cost-effective to reuse solvents rather than discard them when each batch of nanomaterials is synthesized. The mechanistic study allowed for the recycling of the solvent used for synthesizing various Fe_3O_4 nanocrystals. In this study, the supernatant from a previous process was retained and then used for the subsequent preparation of porous Fe_3O_4 nanocrystals composed of small grains. When the nanoparticle is interconnected with small grains, this nanoparticle is generally denoted as a porous nanoparticle.[23,24] A mixture of $Fe(acac)_3$ (100 g) and the first recycled solvent (the first supernatant) was heated to 300°C and maintained at this temperature for 30 min. As much as 20.9 g of nanocrystals were produced at a yield of 95%. Figure 5(a) shows a TEM image of the quasicubic Fe_3O_4 nanocrystals with an average size of 25 ± 2.7 nm, and the porous Fe_3O_4 nanocrystals are constructed from interconnected nanograins. The lattice spacing of the Fe_3O_4 shown in the HRTEM image [Fig. 5(a) inset] was approximately 0.295 nm ((220) plane). The XRD patterns of the Fe_3O_4 nanocrystals are shown in Fig. 5(b). The diffraction peaks were also indexed to the magnetite phase (JCPDS No. 71-6336). An analogous synthetic procedure was used in a subsequent preparation using the second recycled solvent (the second supernatant), which was the solvent collected from the quasicubic Fe_3O_4 nanocrystals, which also afforded porous Fe_3O_4 nanocrystals composed of many interconnected nanograins. Figure 5(c) shows a TEM image of Fe_3O_4 nanocrystals with an average size of 36 ± 3.2 nm, regular pores, and multigrain nanocrystals. The Fe_3O_4

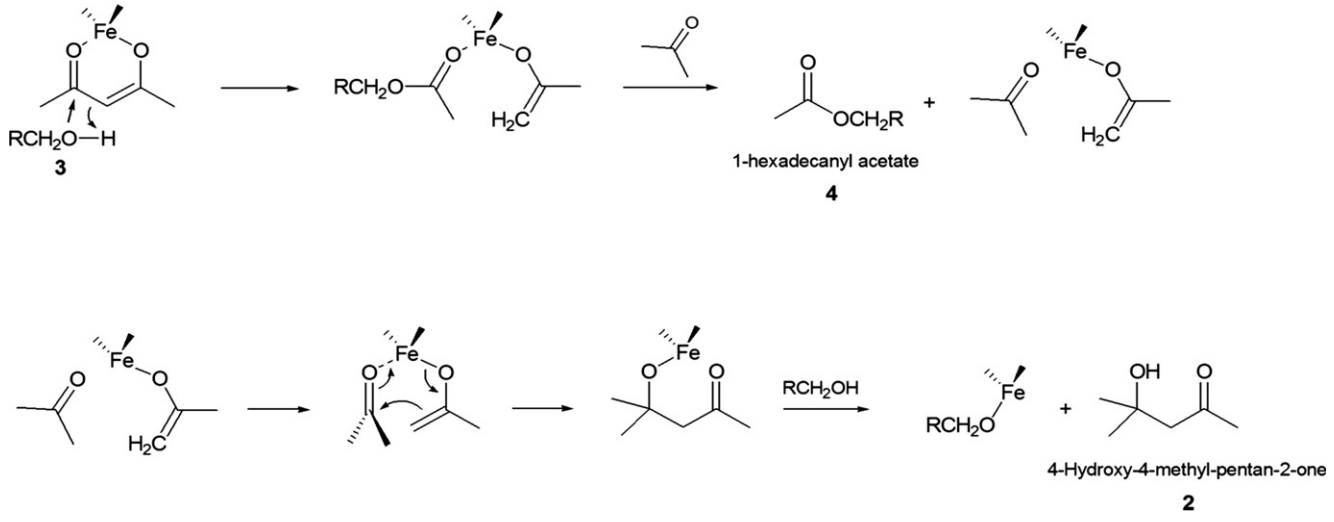

Fig. 2. Schematic view of reaction pathways for the formation of Fe_3O_4 nanocrystals in the presence of 1-hexadecanol (RCH_2OH).

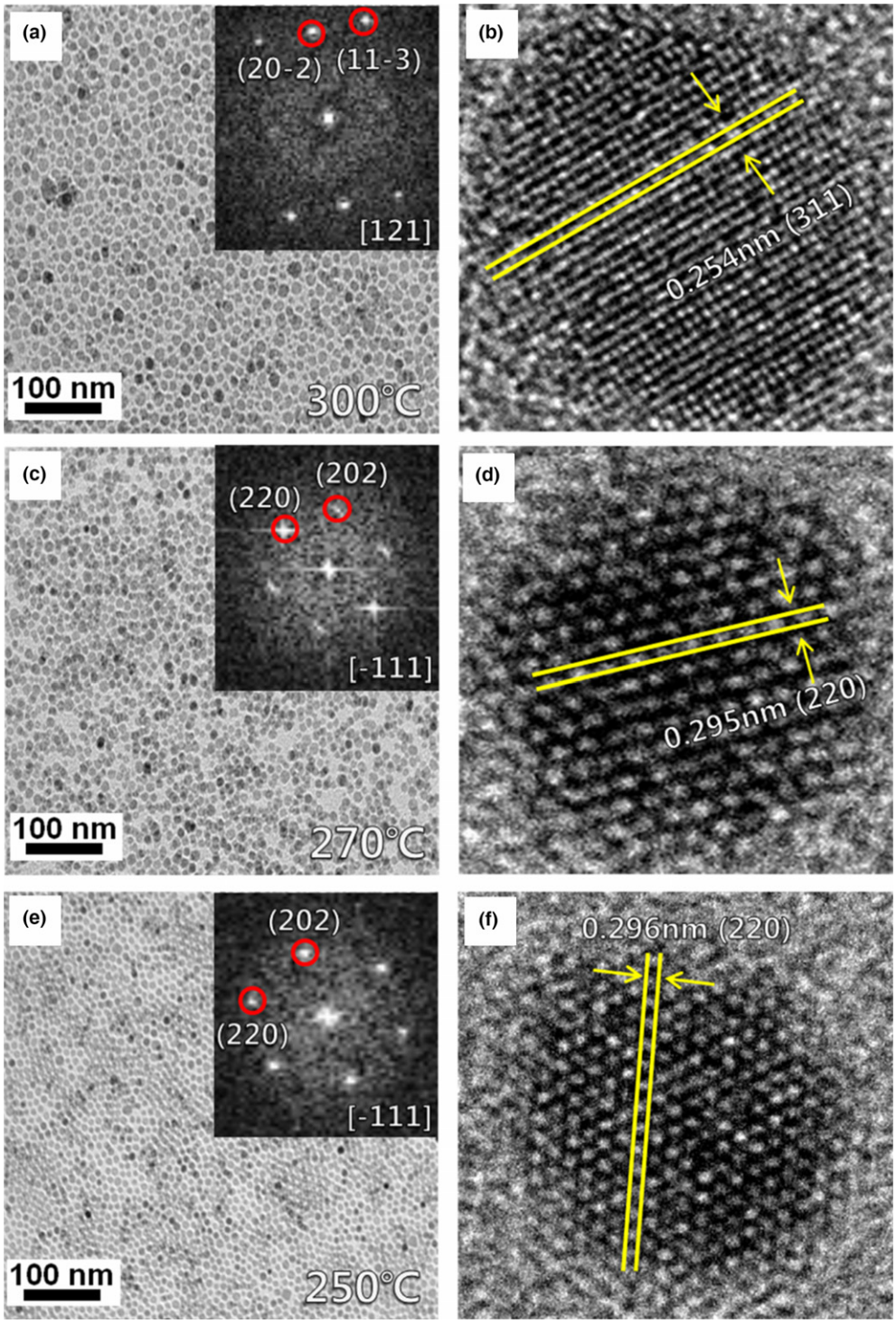

Fig. 3. TEM micrographs and FFT patterns of the Fe_3O_4 nanocrystals. [(a), (c) and (e)] TEM and [(b), (d) and (f)] HR-TEM images of Fe_3O_4 nanocrystals with an average size of [(a) and (b)] 7.8 ± 0.6 nm, [(c) and (d)] 6.5 ± 0.4 nm, and [(e) and (f)] 5.9 ± 0.2 nm. FFT patterns (inset) obtained using a Digital Micrograph with the corresponding areas in (b), (d), and (f).

shown in the HR-TEM image in Fig. 5(c) (inset) had lattice spacing of approximately 0.291 nm ((220) plane) and 0.251 nm ((311) plane) and displayed small grain boundaries. The only experimental difference in this durable procedure was the presence of (4) in the solvent used, which resulted in the formation of nanocrystals with larger diameters and pores. The GC-MS results in Fig. 6 show a gradual increase in the ratio (4)/(3) from 2.8 to 22.4 during the reaction process, which matched well with increasing particle sizes. The color of the reaction mixture changed from red color for the iron precursor to black for the Fe_3O_4 nanocrystals during the synthesis of Fe_3O_4 nanocrystals. This color change was a good indicator of the reaction's progress. As the amount of (4) increased in the mixture, the color change from red to black proceeded more slowly, suggesting that the rate of Fe_3O_4 seed formation was significantly diminished. This phenomena indicate that the presence of (4) diluted the reaction solvent (surfactant), 1-hexadecanol, resulting in the formation of larger Fe_3O_4 nanocrystals. Generally, lower concentration of surfactant tends to produce bigger nanopartices.[21] However, it is not clear whether (4) inhibited the formation of Fe_3O_4

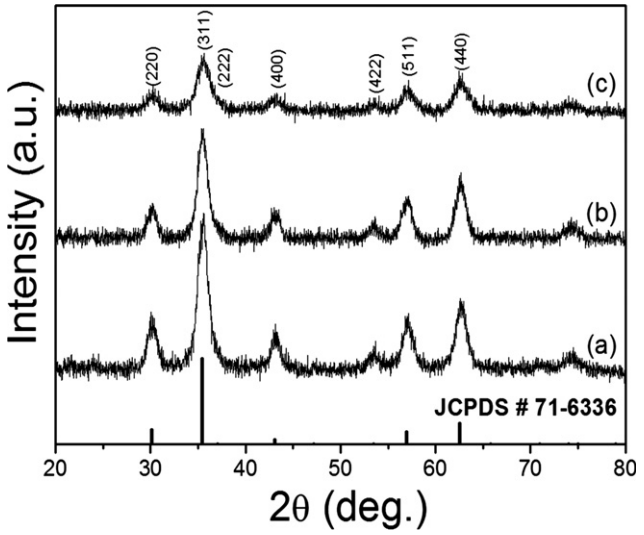

Fig. 4. XRD patterns of Fe_3O_4 nanocrystals synthesized at reaction temperatures of (a) 300°C, (b) 270°C, and (c) 250°C.

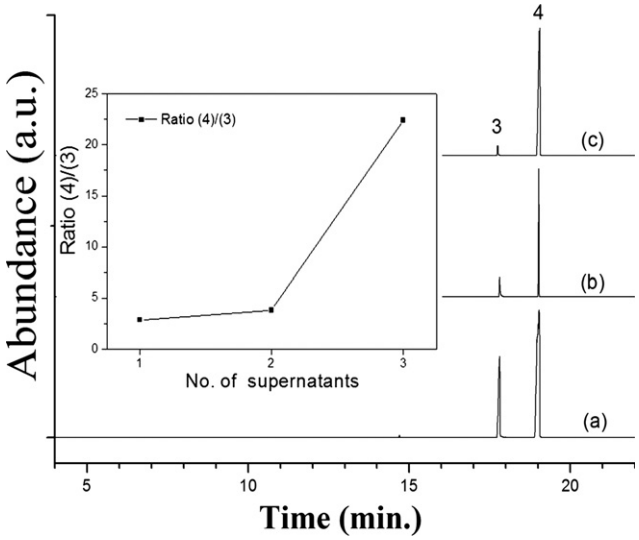

Fig. 6. Gas chromatograms of (a) the first supernatant, (b) the second supernatant, and (c) the third supernatant. The inset shows a ratio of (4)/(3).

seeds or played a more active role in the thermal decomposition kinetics. A more quantitative analysis is necessary to make this determination.

The physicochemical properties are related to many elements such as morphology, crystallinity, and crystal defects.[25,26] The magnetic properties of Fe_3O_4 nanocrystals depending on the morphologies were characterized by the vibrating sample magnetometer (VSM) at 300 K (Fig. 7). As expected, the Fe_3O_4 nanocrystals showed typical ferromagnetic behaviors. The coercivity values for the Fe_3O_4 nanocrystals of 7.8 ± 0.6 nm and porous Fe_3O_4 nanocrystals (25 ± 2.7 and 36 ± 3.2 nm samples) were 67.32, 81.23, and 91.54 Oe, respectively. Besides, the Fe_3O_4 nanocrystals have

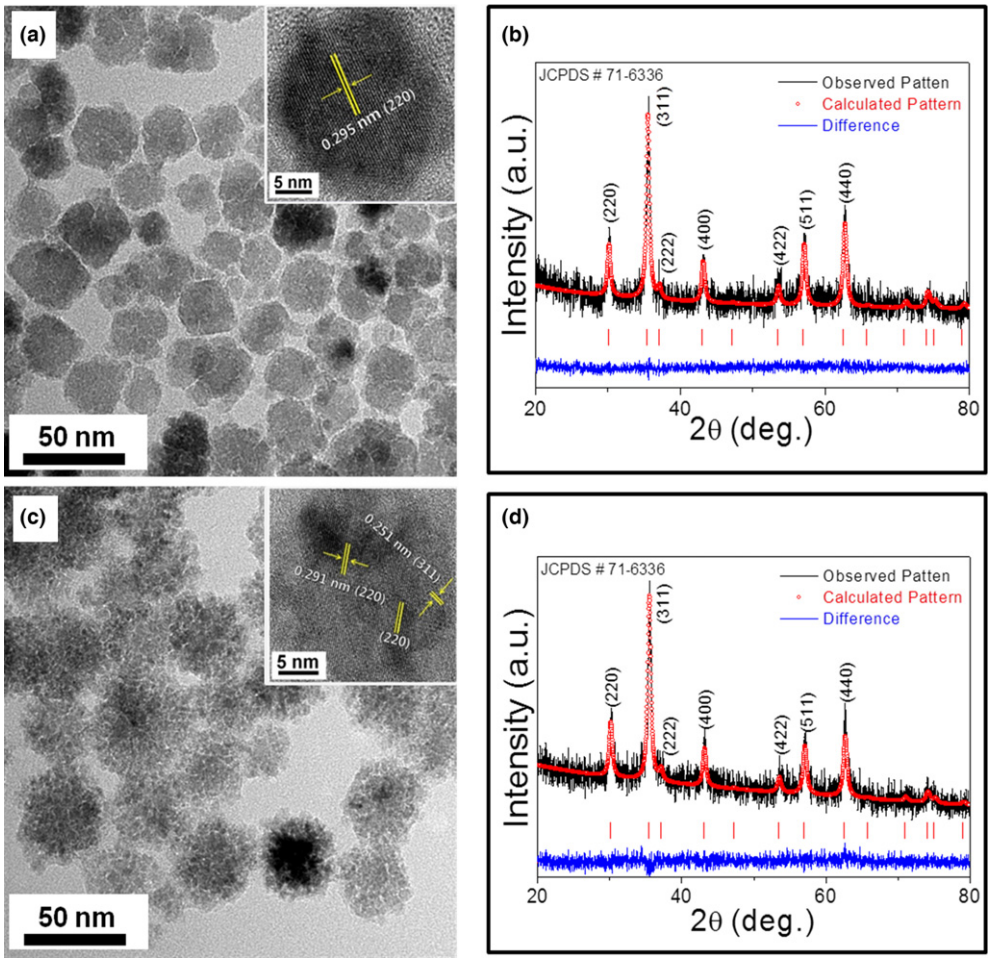

Fig. 5. [(a) and (c)] TEM images and [(b) and (d)] XRD patterns of porous Fe_3O_4 nanocrystals prepared using recycled solvent with average sizes of [(a) and (b)] 25 ± 2.7 nm and [(c) and (d)] 36 ± 3.2 nm.

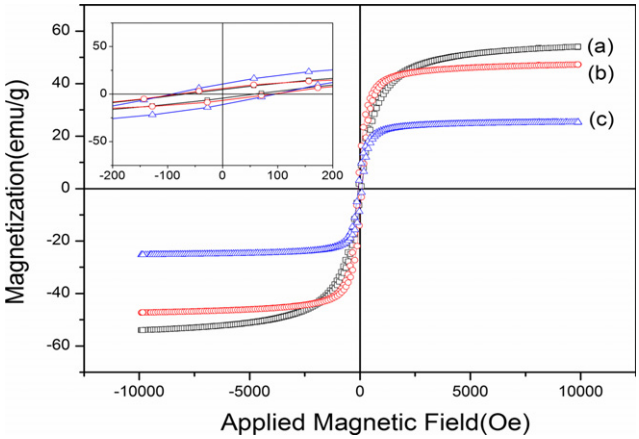

Fig. 7. Magnetic hysteresis loops of (a) Fe_3O_4 nanocrystals (average size of 7.8 ± 0.6 nm), and porous Fe_3O_4 nanocrystals of average size of (b) 25 ± 2.7 and (c) 36 ± 3.2 nm.

low remanence values of about 4.78, 5.97, and 10.5 emu/g. Generally, the saturation magnetization (M_S) is expected to increase with an increasing particle size.[22,25,26] However, the M_S value of porous Fe_3O_4 nanocrystals decreased with the increasing particle size of the nanocrystals. The M_S values of porous Fe_3O_4 nanocrystals (25 ± 2.7 and 36 ± 3.2 nm samples) roughly accounts for 51% (47.22 emu/g), and 27% (25.25 emu/g) of the corresponding bulk value (92 emu/g). This unusual behavior seems to be attributable to the porous nature of our Fe_3O_4 nanocrystals. The M_S values were commonly reported to be smaller (by 20%–25%) for hollow nanoparticles than those for the bulk.[15] Ongoing work will involve an investigation of the detailed formation mechanisms and magnetic properties of porous Fe_3O_4 nanocrystals.

IV. Conclusion

We reported a facile process for the synthesis of Fe_3O_4 nanocrystals via the thermal decomposition of $Fe(acac)_3$ in 1-hexadecanol. Formation mechanisms were elucidated on the basis of GC-MS analysis, which enabled large-scale nanocrystal preparation. The resulting nanocrystals had a spherical shape with average diameters of 7.8 ± 0.6, 6.5 ± 0.4, and 5.9 ± 0.2 nm when prepared at 300°C, 270°C, and 250°C, respectively. This synthetic method had a high yield and good reproducibility. Furthermore, to demonstrate economical application, porous Fe_3O_4 nanocrystals were prepared using recycled solvent, which was recovered from previous processes. The resulting Fe_3O_4 nanocrystals with porous structures had larger average sizes of 25 ± 2.7 and 36 ± 3.2 nm than those obtained from the initial process. These results indicate a promising durable route for the large-scale preparation of nanocrystals with controlled sizes and morphologies.

Acknowledgments

We acknowledge KBSI grants (no. C36957) for financial support of this project. This work was supported by Small and Medium Business Administration (S2060417) and the Basic Science Research Program through the National Research Foundation of Korea (NRF) funded by the Ministry of Science, ICT & Future Planning (NRF-2015R1C1A1A02037373, NRF-2014R1A6B1A01048313, and NRF-2013R1A2A2A01067144).

Supporting Information

Additional Supporting Information may be found in the online version of this article:

Fig. S1. Photographs of experimental procedure for large-scale synthesis of the Fe_3O_4 nanocrystals. (a) the mixture of $Fe(acac)_3$ (100 g) and 1-hexadecanol (409 g) in 2 L glass beaker at room temperature, and (b) the set-up for thermal decomposition reaction (300°C).

Fig. S2. Photographs of (a) the produced nanocrystals of 20.3 g and attraction of (b) the powder and (c) nanoparticles dispersed in toluene by external magnetic field.

Fig. S3. Gas chromatogram of the solvent (1-hexadecanol) from Sigma-Aldrich without further purification. The products are as follows: (1) 16-hydroxyhexadecanoic acid, and (3) 1-hexadecanol.

Fig. S4. TEM images and particle size distribution histograms of Fe_3O_4 nanocrystals with an average size of (a) 7.8 ± 0.6 nm, (b) 6.5 ± 0.4 nm, and (c) 5.9 ± 0.2 nm.

Fig. S5. SAED pattern of the 7.8 nm-sized Fe_3O_4 nanocrystals.

Fig. S6. Rietveld refinement patterns of the 7.8 nm-sized Fe_3O_4 nanocrystals using X-ray powder diffraction. Black solid line represent the observed pattern, and the red dot mark(o) is calculated result. The difference plot (blue) is shown at bottom. Tick marks indicate the reflection positions, which are identified by Rietveld analysis. The published crystal structure of Fe_3O_4 was employed as a starting structural model (ICSD # 6534).

Table S1. Refined crystal structural parameters of Fe_3O_4 nanocrystals obtained from the Rietveld refinement using X-ray powder diffraction data at room temperature. The symbols, *O* and *B*iso, represent the occupation and isotropic thermal parameters, respectively. The numbers in parentheses are the estimated standard deviations of the last significant figure.

References

[1]M. V. Rdddy, G. V. Subba Rao, and B. V. R. Chowdari, "Metal Oxides and Oxysalts as Anode Materials For Li Ion Batteries," *Chem. Rev.*, **113** [3] 5364–457 (2013).
[2]Y.-W. Jun, J.-S. Choi, and J. Cheon, "Shape Control of Semiconductor and Metal Oxide Nanocrystals Through Nonhydrolytic Colloidal Routes," *Angew. Chem. Int. Ed.*, **45** [21] 3414–39 (2006).
[3]A. Kudo and Y. Miseki, "Heterogeneous Photocatalyst Materials for Water Splitting," *Chem. Soc. Rev.*, **38** [1] 253–78 (2009).
[4]S. Laurent, D. Forge, M. Port, A. Roch, C. Robic, et al., "Magnetic Iron Oxide Nanoparticles: Synthesis, Stabilization, Vectorization, Physicochemical Characterizations, and Biological Applications," *Chem. Rev.*, **108** [6] 2064–110 (2008).
[5]T. J. Daou, G. Pourroy, S. Begin-Colin, J. M. Greneche, C. Ulhaq-Bouillet, et al., "Hydrothermal Synthesis of Monodisperse Magnetite Nanoparticles," *Chem. Mater.*, **18** [18] 4399–404 (2006).
[6]N. Pinna, G. Garnweitner, M. Antonietti, and M. A. Niederberger, "General Nonaqueous Route to Binary Metal Oxide Nanocrystals Involving a C-C Bond Cleavage," *J. Am. Chem. Soc.*, **127** [15] 5608–12 (2005).
[7]M. Barroso, A. J. Cowan, S. R. Pendlebury, M. Gratzel, D. R. Klung, and J. R. Durrant, "The Role of Cobalt Phosphate in Enhancing the Photocatalytic Activity of α-Fe_2O_3 Toward Water Oxidation," *J. Am. Chem. Soc.*, **133** [38] 14868–71 (2011).
[8]U. Sobocan, G. Lee, H.-W. Kang, H. J. Kim, Z. Jaglicic, and J. Dolinsek, "The Nature of Magnetic State of Small Fe_3O_4 Nanoparticles," *J. Analytical. Sci. Technol*, **2** [Suppl. A] A8–14 (2011).
[9]S. Lee, H.-W. Kang, M. Kwak, Y.-J. Lee, G. Lee, et al., "Indentification of Spinel Iron Oxide Nanoparticles by ^{57}NMR," *J. Analytical. Sci. Technol*, **2** [Suppl. A] A81–7 (2011).
[10]H. M. Rietveld, "Line Profiles of Neutron Powder-Diffraction Peaks for Structure Refinement," *Acta Crystallogr*, **22** [1] 151–2 (1967).
[11]AXS Bruker, *TOPAS V2.0: General Profile and Structure Analysis Software for Powder Diffraction Data*; User Manual. Bruker AXS, Karlsruhe, Germany, 2000.
[12]A. Kern, A. A. Coelho, and R. W. Cheary, "Convolution Based Profile Fitting"; pp. 17–50 Chapter 2 in *Diffraction Analysis of the Microstructure of Materials*, Edited by E. J. Mittemeijer and P. Scardi. Springer, Berlin, Germany, 2004.
[13]R. W. Cheary and A. Coelho, "A Fundamental Parameter Approach of X-ray Line-Profile Fitting," *J. Appl. Cryst*, **25** [2] 109–21 (1992).
[14]J. Park, K. An, Y. Hwang, J.-G. Park, H.-J. Noh, et al., "Ultra-Large-Scale Syntheses of Monodisperse Nanocrystals," *Nat. Mater.*, **3** [12] 891–5 (2004).
[15]K. M. Nam, J. H. Shim, H. Ki, S.-I. Choi, G. Lee, et al., "Single-Crystalline Hollow Face-Centered-Cubic Nanoparticles From Solid Face-Centered-Cubic Oxide Nanoparticles," *Angew. Chem. Int. Ed.*, **47** [49] 9504–8 (2008).
[16]J. H. Shim, K. M. Nam, W. S. Seo, H. Song, and J. T. Park, "The Role of Water for the Phase-Selective Preparation of Hexagonal and Cubic Cobalt Oxide Nanoparticles," *Chem. Asian J.*, **6** [6] 1575–81 (2012).

[17]M. Niderberger, "Nonaqueous Sol-gel Routes to Metal Oxide Nanoparticles," *Acc. Chem. Res.*, **40** [9] 793–800 (2007).

[18]Y. Sun, Y. Yin, B. T. Mayers, T. Herricks, and Y. Xia, "Uniform Silver Nanowires Synthesis by Reducing $AgNO_3$ With Ethylene Glycol in the Presence of Seeds and Poly(Vinyl Pyrrolidone)," *Chem. Mater.*, **14** [11] 4736–45 (2002).

[19]S. Sun, H. Zeng, D. B. Robinson, S. Raoux, P. M. Rice, et al., "Monodisperse MFe_2O_4 (M = Fe, Co, Mn) Nanoparticles," *J. Am. Chem. Soc.*, **126** [1] 273–9 (2004).

[20]X. Lu, M. Liu, R. Qiao, and M. Gao, "Superdispersible PVP-Coated Fe_3O_4 Nanocrystals Prepared by a "One-Pot" Reaction," *J. Phys. Chem. B*, **112** [46] 14390–4 (2008).

[21]K. M. Nam, J. H. Shim, D.-W. Han, H. S. Kwon, Y. Li, et al., "Syntheses and Characterization of Wurtzite CoO, Rocksalt CoO, and Spinel Co_3O_4 Nanocrystals: Their Interconversion and Tuning of Phase and Morphology," *Chem. Mater.*, **22** [15] 4446–54 (2010).

[22]Y. Lv, Y. Yang, J. Fang, H. Zhang, E. Peng, et al., "Size Dependent Magnetic Hyperthermia of Octahedral Fe_3O_4 Nanoparticles," *RSC Adv.*, **5** [94] 76764–71 (2015).

[23]Y.-S. Hu, Y. G. Guo, W. Single, S. Hore, P. Balaya, and J. Maier, "Electrochemical Lithiation Synthesis of Nanoporous Materials With Superior Catalytic and Capacitive Activity," *Nat. Mater.*, **5** [9] 713–17 (2006).

[24]Q. Su, L. Yao, J. Zhang, G. Du, and B. Xu, "In Situ Transmission Electron Microscopy Observation of the Lithiation-Delithiation Conversion Behavior of CuO/Graphere Anode," *ACS Appl. Mater. Interfaces*, **7** [41] 23062–8 (2015).

[25]P. Guardia, B. Batlle-Brugal, A. G. Roca, O. Iglesias, M. P. Morales, et al., "Surfactant Effects in Monodisperse Magnetite Nanoparticles of Controlled Size," *J. Magn. Magn. Mater.*, **316** [2] e756–9 (2007).

[26]M. Y. Zhu and G. W. Diao, "Synthesis of Porous Fe_3O_4 Nanospheres and Its Application for the Catalytic Degradation of Xylenol Orange," *J. Phys. Chem. C*, **115** [39] 18923–34 (2011). □